Answer to Reviewer 1

We thank reviewer 1 for the review and for the helpful and constructive comments. We took nearly all of them into account in preparing a revised version of our manuscript. The specific comments are answered in the following:

Specific Comments:

RC1: 2.0.1 Title

The title more suggests a description of the turbulence and gas fluxes than a new technique of their calibration and assessment. One might onsider something like: "New calibration procedures not requiring dedicated calibration flights for airborne measurement of air-surface exchange developed using the Polar 5 Aircraft during the AirMeth campaigns."

We agree and changed the title to:

New calibration procedures for airborne turbulence measurements and accuracy of the methane fluxes during the AirMeth campaigns

RC1: Since Table 1 concerns itself primarily with the differences between outbound and inbound legs. It would be helpful to have be a separate table in the same format presenting absolute quantities that define the environment of these flights. Some of these already appear in Table 1, but would better fit in this new table. Such quantities include elapsed time to cover the pair of flight legs, the track direction χ_1 *the wind direction, the track length, the magnitudes of* $v_{||}$ *and* $v_\perp$ *and possibly others.*

We added a further table (Table A1) in the appendix listing all suggested quantities for each individual flight leg.

RC1: Is the Δt *column meant to give the difference in travel time between the out and return legs, or is it to give the total elapsed time in traversing both legs: is it* $t_{leg2} - t_{leg1}$ *or is it* $t_{leg2} + t_{leg1}$ *? Later discussion (static pressure precision) suggests it is the latter, but also presents it as a function of position on the track, not a single number as given in Table 1. This could use some clarification in the table caption and text.*

In Table 1 the difference between the mean time of each leg is given. The symbol Δt was misleading, we changed to $\Delta\bar{t}$. This is now clarified in the caption of Table 1. The time duration needed to fly each leg is now also listed in Tabel A1. In the discussion of the static pressure precision the symbol Δt denotes the (position dependent) time difference.

RC1: 2.0.2 Flight altitude

The airspeed of 60 m s^{-1} *was given, but there was only one mention of the height above ground. That was 50 m above ground for the discussion of Figure 7. Since the ability to attribute flux measurements to surface characteristics* *deteriorates with height above ground, this parameter is important and could be included in the recommended (absolute environment) companion to Table 1.*

The low level flights for flux measurements were mostly done at a height of 50 m above ground. We included the averaged height now in the new table A1. For the calibration of the turbulence probe, however, the height has little relevance and we therefore included in that section also some flight legs at greater heights. Those were actually flown to calibrate remote sensing instruments that are not subject of this paper. For the flux analysis, as e.g. presented in the papers of Kohnert et al. (2018) and Serafimovic, et al. (2018), many more legs were used that did not have an immediate successor on the return track.

RC1: 2.0.4 True Airspeed

The primary concern is a lack of clarity in the development of Manuscript Equation (2) for the "Reference ground speed." The point of Manuscript Equation (2) appears to provide a determination of the true airspeed from the GPS/INS independent of the gust probe's measurements under conditions of the special dual-purpose flights. Some clarification would be helpful:

Quantities v_{gi}, $\chi_i, i = 1, 2$ are probably averages of ground speed (magnitude) over their respective tracks (out and back). This should be made explicit. Presumably, the aircraft is on an autopilot rule to maintain airspeed (but not heading) and ground track (but not groundspeed). If so, however, the origin of Equation (2) is not readily discerned. The following assumptions appear to apply given the description of the reverse-track flights:

1. Wind velocity (magnitude and direction) does not change during the reverse-track maneuver.

2. True airspeed (but not heading) is held as near constant as possible, e.g. 60 m s^-1 (by autopilot or by human pilot)

3. Ground-track direction (but not ground-speed magnitude) is defined by a line segment on the surface, which is followed by the aircraft's autopilot (or human pilot) guided by GPS.

4. Averages are taken of airspeed, groundspeed, and the angle $\gamma_i = \chi_i - \Phi_i$ between ground-track direction and aircraft heading for both legs.

Evaluating the "wind triangle" $V = V_g - V_{\text{TAS}}$ (Manuscript Equation 1) for each of the two passes over the ground track is possible using the law of cosines:

$$V_i^2 = V_{gi}^2 + V_{TASi}^2 - 2V_{gi}V_{TASi}\cos\gamma_i \tag{1}$$

where the non-bold characters represent the magnitudes of the bold vectors, and all quantities are understood to be averages over their respective ground tracks (i = 1, 2). Since wind does not change ($V = V_1 = V_2$) the righthand sides of Equation (1) above for i = 1, 2 can be equated, eliminating windspeed as a variable. All other quantities are known from GPS/INS except for $V_{TAS}i, i = 1, 2$. But the airspeed was held near constant allowing the assumption $V_{TAS1} = V_{TAS2} = V_{TASr}$ where V_{TASr} is the reference that should be equal to $\overline{v_g}$ of the Manuscript Equation (2). Solving for V_{TASr} one gets (assuming the algebra was *correct)*

$$V_{TASr} = \frac{V_{g1}^2 - V_{g2}^2}{2(V_{g1}\cos\gamma_1 - V_{g2}\cos\gamma_2)} \quad (2)$$

Equation (2) above bears some resemblance to Manuscript Equation (2), but time did not permit reconciling these two. They appear to have incompatible forms suggesting that the authors used a different development to arrive at the manuscript's Equation (2). Some additional discussion of the assumptions and derivations actually used, in supplementary material if necessary, needs to be given.

We thank the reviewer for pointing out the deficiency of the manuscript in this part. We clarified our assumptions and rephrased the entire derivation of the reference true airspeed. Please refer to the revised manuscript.

Though mathematically correct, Equation (2) of the reviewer leads to problems in the practical use, as a relatively small difference of two larger quantities appears in the denominator. Assymmetries in the measurement inaccuracies then cause large scatter of the result. The ground speed appearing the the square in the numerator is available with a high accuracy by the gps. The true heading direction, however, is less accurate and represents actually the largest uncertainty in the entire wind derivation. Thus, the small difference of the terms involving direction in the denominator leads to large scatter.

RC1: 2.0.5 Angle of attack ...

No action required.

RC1: 2.0.6 Angle of sideslip and Static Pressure Precision ...

No action required.

RC1: 2.0.7 Accuracy of horizontal wind measurement

The $v_{\|}$ *is declared on page 12, line 10 to dominate "by far" the vector wind compared to the* $V_{\perp}$ *component. "By far" should be quantified. Apparently the flight legs were flown as much as possible parallel to the wind, but if that was clearly stated somewhere, I missed it.*

The formulation was misleading, we rephrased that sentence. We meant an error propagation for the along track component only, as in this component the uncertainty of the dynamic pressure is the major contributer. An error assessment for both wind components is given further down in that section.

RC1: 2.0.8 Methane Analyzer

No action required.

RC1: 2.0.9 Accuracy of methane flux measurements

The precision estimates for the methane flux use a technique described by reference to other publications. I had not seen it before. It looks intriguing. It *would help the moderately interested reader (who can't justify digging through the references) to have a summary of the method. I's not intuitive how one gets a variance of noise error from a cross covariance input. Nor is it described how one finds the standard deviation over the blue-shaded areas. At the very least, the symbols C_{11} and p could be defined with indication of how to compute them. Perhaps C_{11} is the autocovariance of the methane signal with itself and p is the lag?*

We added in the revised manuscript brief summaries of the methods cited and used to assess the instrumental noise and the flux detection limits. Further, we added the missing explanations of the symbols and how to calculate the standard derivation that is now marked in the figure (was Figure 6, now Figure 7).

RC1: 2.0.11 Dry mole fraction flux

Because the methane instrument and the water instrument did not share the same cell in the first two years, it was necessary to use different versions of the WPL terms. The approach looks sound, but the notation suggests some possible problems, hopefully more apparent than real. Page 17, equation (16): The usual expression from WPL in the notation of this manuscript is $\overline{(w\rho_a)' CH'_{4d}}$, where ρ_g is the density of the fraction of "dry" air. This computes the molar flux of CH_4 as the average of the product of the following departure quantities: the molar flux of dry air (as departure quantity $(w\rho_a)'$) times the dry-air mixing ratio of methane (as departure quantity CH'_{4d}). If ρ'_{CH4d} is intended to be defined as $\rho'_a CH'_{4d}$ then it does not separate out the dry-air mass flux $(w\rho_a)'$ which is inconsistent with the method of WPL. Otherwise this section is an informative exploration of the significance of the WPL correction for methane flux in the arctic and an effective demonstration of the effect on the uncertainty when different sensors for water vapor and methane must be used.

The reviewer pointed to a slight inconsistency in the notation. We intended ρ_{CH4d} to be defined as the density of methane. We now dropped the subscript d in the revised manuscript to be consistent with the following formulas.

The technical corrections have all been applied.

Answer to Reviewer 2

We thank reviewer 2 for the review and for the helpful and constructive comments. We took nearly all of them into account in preparing a revised version of our manuscript. The specific comments are answered in the following:

RC2: 1. General comments .... All equations show a "-" instead of "=".

The files uploaded to the copernicus site passed the copernicus validation checks. When downloading the pdf, all equations are printed correctly. We cannot reproduce that effect. What kind of pdf-viewer did the reviewer use ? The technical editor should look into that issue.

RC2: 2. Instrumentation

No action required.

RC2: 3. Calibration of TAS The assumption of the wind changing by less than 0.25 m/s should be addressed more detailed. Which time period is considered? It is unlikely that the wind remains constant over the leg distance of the more than 150 km (first data in table 1). The derivation of equation (2) is missing. I understand this value not as ground speed but corrected speed in aircraft longitudinal direction. So the label of the value v_g is confusing. It might be easier to perform an addition of the two vectors V_g and V (as in equation (1)) to get the reference speed for the TAS calibration. The accuracy of this method is highly depending on the constancy of the wind. A constant change during the two legs seems to stay undetected as this could not be found in the differences of mean values in table 1. Each leg should be analysed separately with respect to time. A standard deviation per leg would be helpful to address this point. Equation (5) implies that the total pressure is measured correctly by the 5-hole probe and the error is only occurs in the static port of this probe. This is not a valid assumption for this kind of probe unless the flow angle at the probe is zero. As the flow angle at the probe is not mentioned a typical calibration curve of the 5-hole probe should be taken into account. The requirements to speed constancy are not mentioned at all. In principle the wind measurement should be independent of TAS but problems might arise by the fact that two legs are averages separately. What happens if one leg is flown at a different speed? The authors should address this point. It is not mentioned whether the computed values for wind and their differences in table 1 are obtained before calibration or thereafter. The major question is the constancy of the wind during the whole roundtrip. What is the influence of a change in the wind over time and how can it be detected and eliminated?

The calibration method does not require a wind changing less than 0.25 m/s for each of the out- and return-flight manoeuvres. We rather argue that with the multitude of such manoeuvres possible wind changes between out- and return flight are randomly distributed and their influence on the eventual calibration parameter is considerably reduced due to the averaging process.

We now more explicitely show the derivation of Equation (2) and rephrased the entire derivation of the reference true airspeed. Please refer to the revised manuscript. We also changed several symbols especially that referring to the reference true airspeed.

The accuracy of this method ist not highly dependent on the wind being constant for each individual pair of return track manoeuvres, as we use a large number of those manoeuvres to find the calibration parameters. There are some manoeuvres (e.g. #1, #4 and #14, we added a sequential numbering in table 1 in the revised version of the manuscript) where the wind changes by about -0.6 m/s or -0.8 m/s between out and return flight. Most manoeuvres, however, have a wind change of about ±0.2 m/s and the average of all changes is -0.11 m/s.

The reviewer correctly pointed out a deficiency in our correction of the static pressure measurements. We now include the probe's error as a function of probe angle as found by wind tunnel tests of an identical model. For most situations of level flights this correction term, however, is very small.

The out- and return flights have been flown at the same manually controlled airspeed. The actual differences in airspeed between both legs are very small. We now include the true airspeed in Table 2, the list of parameters for each separate flight leg.

The computed values listed in Table 1 (and also those in the new Table 2) are calculated after the calibration. This is now mentioned in the table headings.

RC2: 4. Angle of attack calibration The method of angle of attack calibration is described in detail with sufficient explanations. The results are good especially as the flight condi- tions at low level over open sea are ideal. The comparison with the second method is very helpful und shows the effectiveness of both approaches.

No action required.

RC2: 5. Angel of sideslip calibration The derivation of equation (11) is missing. For the sideslip angle calibration the same principle problem occurs as for the TAS calibration: a change of wind and / or TAS over time. An increased wind on one leg will lead to an increased residual error of the sideslip angle. This problem cannot be solved by this method unless the wind and TAS remain constant.

We added further to the derivation of Equation (11) (now Equation 13). The reviewer correctly pointed out, that for a single pair of out- and retur-flights no distinction can be made between a change of wind and a possible misalignment of the probe. However, with a large number of return manoeuvres in different situation and on different days we can assume that possible wind changes are randomly distributed, and thus wind contribution to the average of all residuals (the beta misalignments) should vanish. We further explained this in the revised version of the manuscript.

RC2: 6. Static pressure precision The assessment of static pressure precision *can only refer to a relative accuracy of the measurement. This is not addressed clearly. It is an interesting approach based on statistical methods.*

This is true. Offset errors in the static pressure cannot be detected by this method. We added this comment in the revised manuscript.

~~The Polar 5~~ New calibration procedures for airborne ~~measurement of~~ turbulence measurements and accuracy of the methane fluxes during the AirMeth campaigns

Jörg Hartmann[1], Martin Gehrmann[1], Katrin Kohnert[2], Stefan Metzger[3,4], and Torsten Sachs[2]

[1]Alfred Wegener Institute, Helmholtz Centre for Polar and Marine Research, Bremerhaven, Germany
[2]GFZ German Research Centre for Geosciences, Telegrafenberg, 14473 Potsdam, Germany
[3]National Ecological Observatory Network, Battelle, 1685 38th Street, Boulder, CO 80301, USA
[4]University of Wisconsin-Madison, Dept. of Atmospheric and Oceanic Sciences, 1225 West Dayton Street, Madison, WI 53706, USA

Correspondence to: Jörg Hartmann (Jorg.Hartmann@AWI.de)

June 14, 2018

Abstract.

Low level flights over tundra wetlands in Alaska and Canada have been conducted during the AirMeth campaigns to measure turbulent methane fluxes into the atmosphere. In this paper we describe the instrumentation and new calibration procedures for the essential pressure parameters required for turbulence sensing by an aircraft that exploit suitable regular measurement flight legs without the need for dedicated calibration patterns. We estimate the accuracy of the mean wind and the turbulence measurements. We show that airborne measurements of turbulent fluxes of methane and carbon dioxide using cavity ring down spectroscopy trace gas analysers together with established turbulence equipment achieves a relative accuracy similar to that of measurements of sensible heat flux if applied during low level flights over natural area sources. The inertial subrange of the trace gas fluctuations cannot be resolved due to insufficient high frequency precision of the analyser but since this scatter is uncorrelated with the vertical wind velocity, the covariance and thus the flux is reproduced correctly. In the covariance spectra the -7/3 drop-off in the inertial subrange can be reproduced if sufficient data are available for averaging. For convective conditions and flight legs of several tens of kilometers we estimate the flux detection limit to about 4 mg/m^2/d for $\overline{w'CH_4'}$, 1.4 g/m^2/d for $\overline{w'CO_2'}$, and 4.2 W/m^2 ~~/s~~ for the sensible heat flux.

1 Introduction

The atmospheric methane concentration has nearly tripled since pre-industrial times and is currently rising faster than at any time in the past two decades (Saunois et al. , 2016). Saunois, et al. suggest that this recent rise is predominatly biogenic. The contribution of arctic permafrost regions to this rise and to the global budget in general is still largely uncertain, mainly due to the unavailability of direct measurements on a regional scale. Bousquet et al. (2011) identified natural wetlands to be the main contributor to the interannual variability of the global budget. Thawing permafrost in a warming climate may further increase the contribution of the Arctic. Advancing the knowlegde on arctic methane emission is the motivation to obtain airborne flux measurements over arctic permafrost regions.

The development of robust and precise sensors using cavity ring down spectroscopy for trace gas measurement (Baer et al. , 2002) has made direct flux measurements by eddy correlation covariance possible. Throughout the Arctic flux measurements on tower sites have been established, but regional flux estimates for Arctic tundra areas based on extrapolations of these data currently exceed top-down estimates based on satellite data and global models by a factor of two (McGuire et al. , 2012). Measurements by aircraft allow to extend emission studies into a regional scale and have been used to estimate methane by a budget approach (e.g. Karion et al. (2013), Cambaliza et al. (2014), Hiller et al. (2014)) or by inverse modelling (Miller et al. , 2016)).

Airborne measurements of the direct flux requires the combination of a precise turbulence probe and a fast response gas analyser. Only few aircraft are capable yet to conduct methane flux measurements. Wolfe et al. (2017) used a C23 Sherpa and (Desjardins et al. , 2017) Desjardins et al. (2017) a Twin Otter to measure direct methane emission over mid-latitude agricultural areas. Over the Alaskan North Slope Sayres et al. (2017) and Dobosy et al. (2017) flew a Diamond DA-42 for methane flux measurements. Specifically, eddy-covariance data from low-level flights can be used to create flux maps by means of direct surface projection (e.g. Mauder et al. (2008), Kohnert et al. (2017)) and data fusion (e.g. Metzger et al. (2013), Serafimovich et al. (2018)). These gridded fluxes provide unique insights into the spatial patterning of surface emissions including the location of hot-spots, in a format most suitable e.g. for use with other spatial datasets and model validation.

Airborne turbulence measurements require a calibration of the inherent modification of the surrounding pressure field by the aicraft. For flux and flux map studies flight legs at constant level and constant speed are typically flown and the primary accuracy requirements are on the horizontal wind vector for footprint determination and on the vertical wind for covariances with scalars (temperature, trace gas concentration). We focus in this paper on the calibration for low level runs with approximately constant speed. As many research aircraft are used for mutiple tasks, equipment is not permanently installed and a recalibration is necessary for each re-installation adding extra flight hour requirements per campaign. Here we show some new aspects on inflight calibration using regular flux flight legs to find the primary calibration parameters without additional dedicated calibration patterns.

The aim of the AirMeth campaigns is to obtain measurements of methane emissions from natural area sources to close the gap between bottom-up and top-down estimates of the contribution of Arctic wetlands to the global methane budget. After a few flights in 2011 over northern Germany and Fennoscandia, campaigns were carried out in 2012 and 2013 over the Alaskan North Slope and over the Mackenzie Delta in convective boundary layer conditions. Low level flight legs of 50 to 150 km length were combined with ascents and descents to well above the boundary layer at each end. In each of the latter campaigns some 40 hours of low level legs were flown. Figure 1 shows a typical flight pattern over the Mackenzie Delta. In this paper we describe the instrumentation, calibration procedures and the accuracies of the wind and flux measurements. Analyses of flux patterns, footprint calculations and correlations between fluxes and surface conditions are discussed in Kohnert et al. (2017) and Serafimovich et al. (2018).

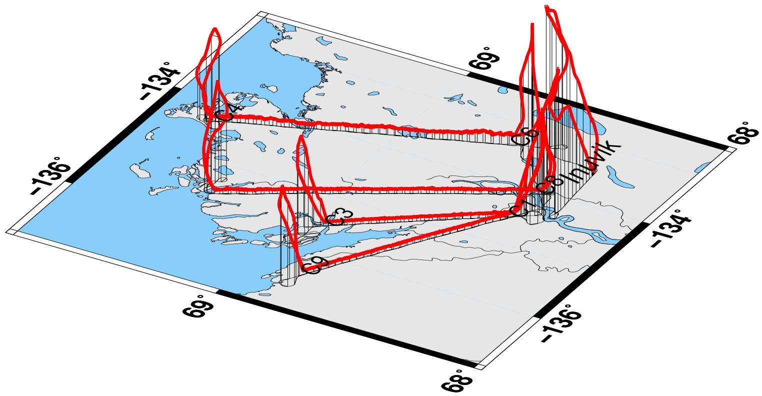

Figure 1. Flight path (solid red) of Polar 5 on 2013-07-20 during the AirMeth campaign illustrating a typical pattern flown with low level return track flight legs and ascents and descents for profiling the convective boundary layer.

Figure 2. Polar 5 during a flight configured for turbulence measurements.

2 Aircraft and instrumentation

The airborne platform we describe in this paper is the AWI (Alfred Wegener Institute) research aircraft Polar 5, a former DC 3, converted by Basler to a turboprob aircraft and now referred to as a BT 67. Polar 5 is unpressurised, able to fly at reasonably low speed (60 m/s for low-level flux measurements, ma≈0.2) and has an endurance of 5 to 6 hours. Figure 2 shows a picture of Polar 5 with the noseboom for turbulence measurements. Polar 5 is used for geosciences and atmospheric measurements and occasionally for logistics (Wesche et al. , 2016). Equipment is not permanently installed and mostly campaigns are flown with different instrumentation. Therefore the calibration coefficients and alignment offsets for the 5-hole-probe are reexamined for each reinstallation. In this paper all instrument description refer to the configuration flown in the 2012 and 2013 AirMeth campaigns.

2.1 Turbulence probe

For turbulence measurements Polar 5 can be equipped with a noseboom carrying a 5-hole probe Type Rosemount 858. The tip of the probe is 2.9 m ahead of the tip of the fuselage. Dynamic, static and the differential pressures are measured by Rosemount pressure transducers. For the static pressure: Rosemount 1201F2A1B1B with a precision better than 0.1 hpa between 200 and 1100 hpa, for the dynamic pressure: Rosemount 1221F2VL6B1B with a precision better than 0.02 hpa for ±50hpa and for the flow angle differential pressures: Rosemount 1221F2VL3B1B with a precision better than 0.01 hpa for ±20hpa. These precisions have been confirmed in laboratory calibrations with temperature variations between 0 and 20°C and during ground recordings with the probe covered. The sensor head of the noseboom is manufactured by MessWERK (Cremer , 2008). The frequency response of the pressure transducers is sufficiently fast for atmospheric turbulence measurements as Lee (1993) found that for frequencies below 1 kHz any difference between source and measured signal cannot be attributed to the pressure sensors.

2.2 Position and velocity

For position, movement and attitude we use a combination of GPS and INS. The INS (inertial navigation system), a Honeywell Laseref V provides the position (longitude, latitude) at 12Hz, the ground speed (v_g), true track angle (χ) and true heading (Ψ) at 25Hz, the pitch (Θ) and roll (Φ) angles at 50Hz and the angular rates at 100Hz. The accuracies for the angles, valid during all flight manoeuvres are gives as $0.1°$ for pitch and roll and $0.4°$ for true heading. The precision of the INS output data depends on the magnitude of flight manoeuvres (e.g. accelerations and turns). A comparison with a GPS derived direction showed $\sigma_\Psi < 0.1°$ during a long straight and level flight. The response time of the INS is 0.02s (as given by the manual) with a delay time of about 0.01s. We found the time difference of 0.03s between INS and GPS by a cross correlation analysis of the velocity components, high-pass filtered with a cut-off at 0.001 Hz. The position and the velocity vector are supported by Novatel ~~GPS~~ GPS FlexPak6. We use the Doppler-derived velocities ('Novatel bestvel') with a precision of 0.03m/s at a data rate of 1 Hz. INS and GPS are merged by complementary filtering at a frequency of 0.1 Hz.

2.3 Temperature and humidity

High speed temperature is recorded by an open wire Pt100 in an unheated Rosemount housing a the tip of the noseboom with a radial distance to the centre of the 5-hole probe of 16 cm and an axial distance of 35 cm. At typical measurement speed of 60 m/s the axial distance corresponds to a time lag of less than one sample at the recording frequency of 100 Hz. The effect of adiabatic heating due to the dynamic pressure has been taken into account. Humidity measurements are provided by a Vaisala HMT-333 mounted in a Rosemount housing in a similar relation to the 5-hole probe as the fast Pt100. The HMT-333 consists of a humicap and a temperature sensor in close connection. This combination allows a correction of the humidity measurement for adiabatic heating. The calibration certificate ~~gives the accuracies~~ provides accuracies of ±0.4% for the relative humidity and of ±0.1°C for the temperature. For cross-checks a Buck-Research CR2 dew point mirror, providing highly accurate but slow absolute values, was mounted in the cabin with an inlet about 6m aft of the 5-hole probe. From 2013 on humidity was also measured in the methane analyser. Polar 5 now also has a Licor 7200, but it was not available in the 2012 and 2013 campaigns.

2.4 Methane analyser

In 2011 and 2012 a Los Gatos LGR Fast Methane Analyser RMT 200 (FMA) was rack mounted in the cabin. The ~~RMT 200~~ FMA has an internal pump enabling a slow operation mode. For flux measurements the airflow through the closed cell sensor was driven by a BOC Edwards XDS35i dry ~~sco1l~~ scroll pump. Outside air was taken in by a rearward facing tube 10cm above the top of the fuselage. To achieve a high flow rate for a fast response we fed the air directly into the analyser using two filters and no air dryer. The air inlet was mounted above the cabin, 7.3m rear of the tip ot the 5-hole probe. 4.3m of stainless steel tubing with an inner diameter of 4mm (which is 54ml of volume) connected the inlet to the ~~RMT~~FMA. In 2013 an LGR-FGGA was used instead of the ~~RMT 200.~~ FMA. All tubing remained unchanged. In addition to CH_4 the FGGA also measured CO_2 and H_2O concentrations.

2.5 Data recorder and sampling frequencies

Polar 5 has a state-of-the-art data aquisition and managment system ("DMS") with a high precision time based on the Precision Time Protocol according to IEEE 1588. The precision of the time stamps of all data is ±60ns, the clock drift less than 1ms over 10h. Time is synchronised to the GPS. The voltage signals of the pressure transducers of the 5-hole-probe and the Pt100 temperature are digitised by 16 bit AD-converters and recorded at 100 Hz. The INS is recorded at the data rates mentioned above via a serial ARINC interface. Relative humidity ~~at 20 Hz serial~~ from the Vaisala ~~interface~~ sensor and the CR2 data ~~also by~~ are recorded via a serial interface at 20 Hz and about 1 Hz, respectively. The methane data are recorded at 16 Hz in internal files by the analyser and additionally the methane concentration is fed into the DMS via an analog signal through the AD-converters to enable synchronisation.

3 Calibration procedures and instrumental alignment

The wind measurement by an aircraft is the usually small difference between two larger vectors: the aicraft vector with respect to Earth $\boldsymbol{V_g}$ and the airflow vector with respect to the moving air $\boldsymbol{V_{\mathrm{TAS}}}$:

$$\boldsymbol{V} = \boldsymbol{V_g} - \boldsymbol{V_{\mathrm{TAS}}} \quad (1)$$

$\boldsymbol{V_g}$ is given with high accuracy by the combination of INS and GPS, $\boldsymbol{V_{\mathrm{TAS}}}$ is based on measurements by pressure sensors at the aircraft and transformed from the aircraft system into the local Earth system by three ~~roations~~ rotations given in e.g. Lenschow and Spyers-Duran (1989), Hartmann (1990). As modifying its surrounding pressure field is the very essence of flying an aircraft heavier than air, all pressure measurements need to be calibrated to account for these modifications. Since flying the aircraft in a wind tunnel is no option we have no other choice as to perform in-flight calibrations.

Calibration manoeuvres are described for single engine aircraft e.g. by Vellinga et al. (2013) and Mallaun et al. (2015) and for twin engine aircraft e.g. by Tjernström and Friehe (1991), Cremer (2008), and Drüe and Heinemann (2013). Typically a constant wind is assumed and speed variations are flown in box or race-track patterns for the calibration of the dynamic pressure and in level flights for the angle of attack α. However, little attention is paid to assess the accuracy of the assumption of a constant wind. We address that problem and describe a calibration procedure that does not need a dedicated flight pattern by exploiting a series of return-track flight legs flown for flux measurements.

3.1 True airspeed (TAS)

We focus on the condition of flux measurement flights, i.e. a true airspeed (TAS) of 60m/s and level flight and use the random variations in the airspeed on manually controlled flights. For an accuracy of the wind measurement better than 0.25m/s the uncertainty in the dynamic pressure needs to be smaller than 0.2hpa. As the absolute wind is virtually never known with this accuracy, we ~~can do with the assumption of the wind changing less than this 0.25m/s during a reverse heading manoeuvre. To further overcome the uncertainty of changes in the wind field during the calibration flight, we use multiple calibration events,~~ perform reverse heading manoeuvres during which the mean wind changes little. Furthermore we use a multitude of these manoeuvres distributed randomly in space~~and time~~ , time and orientation over the course of ~~a campaign, to~~ the campaign. We assume that the small changes of the mean wind that might occur during individual out- and return flights, are uncorrelated between the multiple realisations of these manoeuvres. Averaging over all such pairs of flight manoeuvres will then reduce the uncertainty ~~of the wind assumption~~ in the assumption of a constant wind by $1/\sqrt{n}$, n being the number of such ~~calibration events~~manoeuvres. For example with n=16, we can reduce the wind uncertainty of the calibration procedure by a factor of 4. Of all flight legs during the 2013 AirMeth campaign 15 have been flown in reverse order in immediate succession~~. A list of these pairs of flight legs is given in Table~~, they are listed in Table ~~1.~~ A1.

For a flight track exactly parallel to a constant wind the average of the true airspeed (v_T) of both legs equals the average of the true ground speed (v_g) of both legs:

$$\frac{1}{2}(v_{T1} + v_{T2}) = \frac{1}{2}(v_{g1} + v_{g2}), \tag{2}$$

where the indices 1 and 2 refer to the out- and return flight legs, respectively. For a wind deviating from the parallel to the true ground track, the aircraft heading is turned slightly into the wind leading to a reduced ground speed. Related to this ground speed, the true airspeed is increased by $1/\cos(\gamma)$, with $\gamma = \Psi - \chi$ being the angle between the true heading Ψ and the true track χ. Figure 3 shows a sketch illustrating the angles. For small angles γ and with the assumptions described above, Equation 2 becomes

$$\frac{1}{2}(v_{T1} + v_{T2}) = \frac{1}{2}\left(\frac{v_{g1}}{\cos(\gamma_1)} + \frac{v_{g2}}{\cos(\gamma_2)}\right) = v_{\text{ref}}, \tag{3}$$

with v_{ref} denoting the reference speed for this pair of return flights.

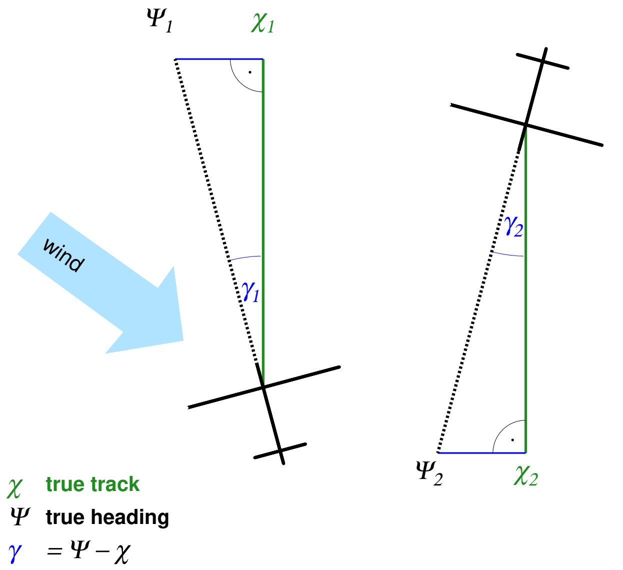

Figure 3. Illustration of the angles true track χ and true heading Ψ for reverse heading flights.

In our case $|\gamma|$ is typically 2-3°, corresponding to values for $1/\cos(\gamma)$ of ≈ 1.001, i.e. the reference ground speed is about 1‰ higher than the true ground speed. With v_{ref} we calculate the reference undisturbed dynamic pressure as

$$q_{\text{ref}} = \frac{1}{2}\overline{\rho}\,\overline{v_{\text{ref}}}^2 \tag{4}$$

with ρ being the air density. Similarly we average the indicated dynamic pressure $q_i = 0.5(q_{i1} + q_{i2})$ and use Eq.(4) to calibrate q_i at the tip of the 5-hole-probe by

$$q_{\text{ref}} = c_q q_i \tag{5}$$

We find that in the range of values realised during typical low level flux runs Equation 5 is best approximated by a linear relationship with $c_q = 1.165$, as shown in Figure 4. The standard deviation of the points (q_c) from the approximation ($1.165q_i$) is 0.014hpa, which we take as an estimate of the calibration accuracy. The static pressure measurement can then be corrected by

$$p_s = p_{si} + q_i(1 - c_q) + \Delta p_s, \tag{6}$$

where Δp_s is the measurement error of the Rosemount probe as a function of the flow angle. We use the wind tunnel measurements done by Mühlbauer (1985) with an identical Rosemount probe to approximate Δp_s by a second degree polynomial:

$$\Delta p_s = (0.0069 - 3.62 \cdot 10^{-5}\phi - 0.0003155\,\phi^2)q_i, \tag{7}$$

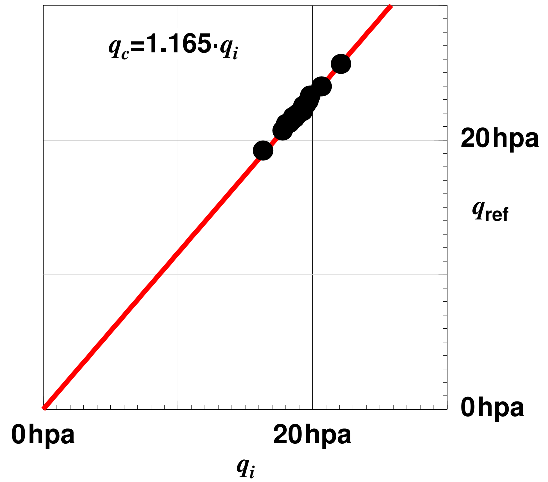

Figure 4. Dynamic pressure derived by Equation 4 versus the indicated dynamic pressure at the tip of the 5-hole-probe. Each of the 15 dots represents the average of two overpasses of the same track in revese direction. The red line is a linear regression.

where ϕ is the flow angle defined by $\cos(\phi) = \cos(\alpha)\cos(\beta)$. For flux measurement runs with α being roughly 5°, Eq. 7 leads to a correction of typically 0.04 hpa.

For each pair we calculate a reference ground speed

$$\overline{v_g} = \frac{1}{2}\left(\frac{v_{g1}}{\cos(\chi_1 - \Psi_1)} + \frac{v_{g2}}{\cos(\chi_2 - \Psi_2)}\right),$$

the indices 1 and 2 refer to the out and return legs, respectively, $(\chi - \Psi)$ is the difference angle between the true track and the true heading, as the aircraft heading deviates somewhat from the track towards the wind direction, resulting in a slightly increased TAS. Figure 4 shows a sketch illustrating the angles. In our case $(\chi - \Psi)$ is typically 2-3°, corresponding to values for $1/\cos(\chi - \Psi)$ of ≈ 1.001, i.e. the reference ground speed is about 1 higher than the true groundspeed. With $\overline{v_g}$ we calculate the reference undisturbed dynamic pressure as

$$q_{gs} = \frac{1}{2}\overline{\rho}\,\overline{v_g}^2$$

with ρ being the air density. Similarly we average the indicated dynamic pressure $q_i = 0.5(q_{i1} + q_{i2})$ and use Eq.(4) to calibrate q_i at the tip of the 5-hole-probe by

$$q_{gs} = c_q q_i$$

We find that in the range of values realised during typical low level flux runs Equation 5 is best approximated by a linear relationship, $c_q = 1.165$, shown in Figure 4. left: illustration of the angles true track χ and true heading Ψ for reverse heading flights. right: dynamic pressure derived by Equation 4 versus the indicated dynamic pressure at the tip of the 5-hole-probe. Each of the 15 dots represents the average of two overpasses of the same track in revese direction. The red line is a linear regression.

Table 1. ~~Horizontal~~ Return track flight ~~legs~~ sections used for the calibration of the dynamic pressure measurement and the alignment between the 5-hole-probe and the INS reference. Each line refers to one pair of return flights over the same track. The first ~~two~~ column is a sequential numbering, the second and third columns give the codes of the flight legs, further details ~~and a full list of all flight legs is given~~ are listed in ~~Kohnert et al. (2014)~~Table A1. ~~l the averaged length, $\overline{v_g}$ the averaged ground speed,~~ Δt is the time difference between ~~both legs~~the middle of each leg, $\Delta\chi$ the difference in the track angle, $\Delta|U|$ the difference in the wind speed, Δu and Δv the differences of the horizontal wind components (u positive to the East and v positive to the North), $\Delta u_\perp$ and $\Delta v_\parallel$ the differences in components of the wind rotated to align with the track angle, and β_r the remaining offset in the β-angle (12). All parameters are calculated after the calibration.

	leg 1	leg 2	~~l $\overline{v_g}$~~ Δt	~~χ_1~~ $\Delta\chi$	$\Delta\|U\|$	Δu	Δv	$\Delta u_\perp$	$\Delta v_\parallel$	β_r
		~~km~~	~~m/~~s	~~s~~ °°	m/s	m/s	m/s	m/s	m/s	°
~~CP50706h02 CP50706h03~~ 1	~~156.1~~ CP507**06h02**	~~56.27~~ CP507**06h03**	3814	~~96.8~~ -0.5	-0.79	-0.79	0.18	0.10	0.81	0.02
~~CP50711L08 CP50711L09~~ 2	~~12.0~~ CP507**11L08**	~~64.68~~ CP507**11L09**	327	~~181.5~~ 0.6	0.20	0.12	0.68	0.16	0.62	0.04
~~CP50712h01 CP50712h02~~ 3	~~90.8~~ CP507**12h01**	~~57.77~~ CP507**12h02**	2122	~~273.6~~ -0.2	0.24	0.24	0.21	-0.27	0.23	-0.07
~~CP50712h03 CP50712h04~~ 4	~~92.4~~ CP507**12h03**	~~58.55~~ CP507**12h04**	2145	~~93.6~~ -0.0	-0.66	-0.65	0.26	0.23	0.67	0.06
~~CP50719h01 CP50719h02~~ 5	~~109.8~~ CP507**19h01**	~~59.62~~ CP507**19h02**	2715	~~338.8~~ -0.1	0.24	0.21	-0.33	-0.11	0.39	-0.03
~~CP50720h01 CP50720h02~~ 6	~~101.0~~ CP507**20h01**	~~58.67~~ CP507**20h02**	2422	~~338.9~~ 0.4	0.29	0.13	0.05	-0.29	0.09	-0.07
~~CP50720h03 CP50720h04~~ 7	~~118.7~~ CP507**20h03**	~~59.49~~ CP507**20h04**	2605	~~330.2~~ -0.1	-0.21	-0.34	0.08	0.14	-0.17	0.03
~~CP50720h05 CP50720h06~~ 8	~~68.9~~ CP507**20h05**	~~60.01~~ CP507**20h06**	1636	~~324.4~~ 0.1	-0.16	-0.27	-0.05	0.16	-0.05	0.04
~~CP50720h07 CP50720h08~~ 9	~~84.3~~ CP507**20h07**	~~60.93~~ CP507**20h08**	1885	~~301.1~~ 0.4	-0.22	-0.30	0.01	0.11	-0.18	0.03
~~CP50721L03 CP50721L04~~ 10	~~12.9~~ CP507**21L03**	~~65.58~~ CP507**21L04**	318	~~360.0~~ -0.3	0.29	0.10	0.24	-0.28	-0.25	-0.06
~~CP50721h01 CP50721h02~~ 11	~~82.5~~ CP507**21h01**	~~62.85~~ CP507**21h02**	2727	~~179.9~~ -0.4	-0.05	0.07	0.07	-0.07	0.08	-0.02
~~CP50721h03 CP50721h04~~ 12	~~98.7~~ CP507**21h03**	~~65.16~~ CP507**21h04**	2125	~~180.1~~ -0.4	-0.14	0.01	-0.09	-0.16	-0.09	-0.04
~~CP50722h04 CP50722h05~~ 13	~~68.8~~ CP507**22h04**	~~61.65~~ CP507**22h05**	1654	~~324.4~~ 0.5	-0.09	-0.15	-0.35	0.32	0.21	0.07
~~CP50723h02 CP50723h03~~ 14	~~86.8~~ CP507**23h02**	~~60.34~~ CP507**23h03**	2065	~~211.9~~ 0.1	-0.66	-0.59	-0.42	-0.34	-0.69	-0.08
~~CP50723h04 CP50723h05~~ 15	~~112.1~~ CP507**23h04**	~~61.59~~ CP507**23h05**	2458	~~209.9~~ 0.0	0.05	0.10	0.05	0.02	0.07	0.01
~~mean~~	~~81.3~~	~~62.98~~ mean	1956	-0.0	-0.11	-0.14	0.04	-0.02	0.12	-0.00
~~σ~~		σ		0.3	0.36	0.33	0.28	0.21	0.39	0.05

~~The standard deviation of the points (q_c) from the approximation ($1.165 q_i$) is 0.014hpa, which we take as an estimate of the calibration accuracy. The static pressure measurement can then be corrected by~~

~~$p_s = p_{si} + q_i(1 - c_q).$~~

3.2 Angle of attack alpha

At the 5-hole-probe a pressure difference results between the two holes in the vertical plane that depends on the angle of attack α. This relation is a function of the shape of the probe and of the aerodynamical influence of the aircraft. The probe's shape has been thoroughly ~~testet~~ tested in wind tunnels e.g. (De Leo and Hagen , 1976) (Mühlbauer , 1985) and analysed theoretically (Rodi and Leon , 2012) to be expressed by a linear proportionality: $\alpha_i \sim q_\alpha / q_i$ with a proportionality constant of 12.67 and α_i being the indicated, i.e. undisturbed, angle of attack, q_α the indicated pressure difference and q_i the indicated dynamic pressure. A small dependence on the Mach number is neglected, since it is about 4 orders of magnitude smaller for the airspeed of our measurement flights. The proportionality constant is valid for a probe in an undisturbed flow, but the influence of the aircraft leads to a deviation from this number. Crawford et al. (1996) explained this deviations in terms of "lift induced upwash" in front of the aircraft. Furthermore the α measurement needs to be aligned with the coordinate system of the INS. This alignment may be different for each re-installation of the noseboom. Therefore an α calibration is typically done for each remounting of the probe and any change in the configuration of the aircraft. We combine the effects of probe shape and aircraft influence in a single calibration procedure. For the small angles that occur during straight level flights α depends with a very good approximation linearly on the pressure difference normalised by the dynamic pressure:

$$\alpha = \alpha_0 + c_\alpha \frac{q_\alpha}{q_i} \tag{8}$$

with α_0 being the offset angle between the 5-hole-probe and the reference of the INS, and c_α the proportionality constant.

3.2.1 Dedicated calibration flight

For a calibration flight pattern we use the fact that a) with no pressure influence by the aircraft the angle of attack α equals the pitch angle during a straight and level flight with no vertical movement of the air and that b) for a plane with fixed aerofoil (no flap movement) α varies with airspeed. This is a very commonly used method for the α-calibration. We performed three low level flight sections over water with the airspeed ~~gradualy~~ gradually increasing from 50m/s to 90m/s during 5 minutes and decreasing back to 50m/s again during 5 minutes. For these data Figure 5 shows pitch versus q_α/q_i. As the aircraft is manually controlled during this manoeuvre and the vertical movement of the air is not constantly zero, points scatter vertically with the vertical speed of the aircraft w_g and horizontally with vertical wind velocity w. The colour coding with w_g shows that most of the scatter in explained by vertical movement of the aircraft. Typically this is being assumed to cancel on average (e.g. Mallaun et al. , 2015) and mean values over subsections are used for the calibration. This implicitely assumes a Gaussian distribution of w and w_g.

With the quite accurate knowledge of w_g we can restrict the data used for a regression to these conditions of very little vertical movement of air and aircraft and level wings, i.e.:

$$|w_g| < 0.05\text{m/s} \;\wedge\; |w| < 0.1\text{m/s} \;\wedge\; |\Phi| < 5^\circ \tag{9}$$

and furthermore correct the pitch angle by

$$\Theta_c = \Theta - \frac{w_g}{\text{TAS}} \frac{180}{\pi} \tag{10}$$

to account for the remaining small vertical movement of the plane to arrive at

$$\alpha_0 = -1.822 \pm 0.033 \quad \text{and} \quad c_\alpha = 10.375 \pm 0.073. \tag{11}$$

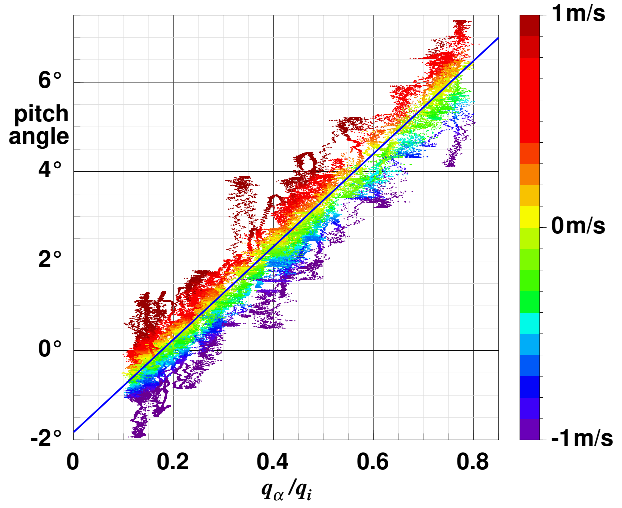

Figure 5. Pitch angle Θ versus alpha pressure difference normalised by the dynamic pressure q_α/q_i. The data are from three low-level calibration flight sections over water off Barrow on 6 July 2013. Colour coded is the vertical velocity of the aircraft w_g with the colour scale given in the vertical bar at the right. Plotted are the 100Hz data. The blue line represents the linear regression $\alpha = -1.822 + 10.375\frac{q_\alpha}{q_i}$.

Note that for our data (Eq. 9) the correction term in (10) is smaller than $0.05°$. As the vertical wind velocity, needed for the selection condition (9), is not known before the final calibration coefficients are determined, we need to run through one step of iteration for which we use the coefficients of the most recent campaign as a first guess. The uncertainties in the regression coefficients in (11) translate into an offset uncertainty for the vertical wind velocity of ~ 0.03m/s and a gain uncertainty of $\sim 0.7\%$. Our value for c_α is close to that of Mallaun et al. (2015) who found a correction factor of 0.78 necessary for theoretical value of 12.66 to account for the aircraft influence of a Cessna Grand Caravan. A Gaussian error propagation for Eq. 8 with q_i=20 hpa (TAS $\approx$ 60 m/s) and q_a=10 hpa (vertical wind $\approx$ 1 m/s) and using the uncertainties $0.033°$ for α_0, $0.073°$ for c_α, 0.01 hpa for q_α and 0.02 hpa for q_i yields an uncertainty for α of $0.05°$, with the dominating contribution from the uncertainty of the regression slope.

3.2.2 No need for calibration flight for α

It is interesting to note that an α calibration is actually possible without any specific flight manoeuvre if sufficient data are available. We demonstrate this for the AirMeth campaign in 2013. We use all flight data of all days, except the 6$^{\text{th}}$ of July 2013, the day of the dedicated α-pattern, to have an independent test. Of these 68 h of flight data (with q_i >10 hpa, $\cong$ 50 m/s to ensure in-flight conditions) we select those that fulfill the conditions given in (9): vertical movement of the plane smaller than 5 cm/s, vertical wind velocity smaller than 0.1 m/s, roll angle smaller than 5° (absolute values for each). Roughly 0.6 % of the data remain and are plotted in Figure 6 as red dots. For comparison grey shading indicates the density distribution of all 68h of data. A least squares fit of a linear relation results in $\alpha_0 = -1.856 \pm 0.016$ and $c_\alpha = 10.449 \pm 0.030$, which are within the range of uncertainty of (11) and differ from the values of the dedicated pattern by 1.8% for the offset and 0.7% for the

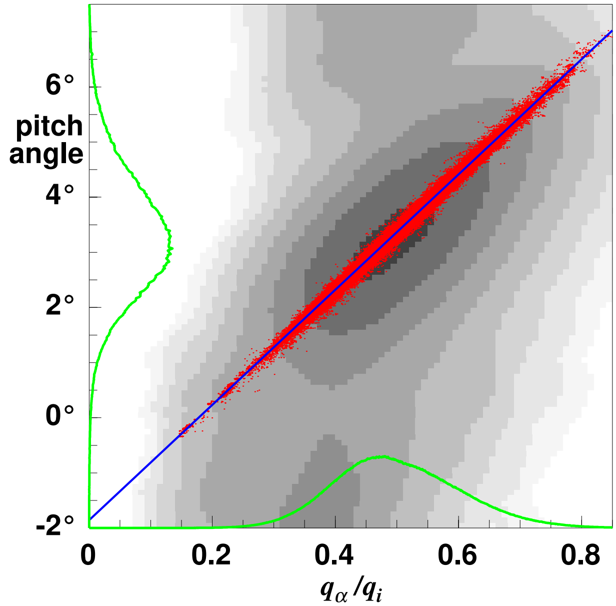

Figure 6. Pitch angle versus alpha pressure difference normalised by the dynamic pressure for all flights (except 6 July 2013) during the 2013 AirMeth campaign. Red dots are data that fulfill the conditions given in (9) and with correction of the pitch angle Eq. (10). Grey shading indicates the distribution of all data which includes ascents, descents, take-off and landing procedures. A logarithmic shading scale is used. Only data with $q_i < 10$hpa (corresponding to TAS=50m/s) are excluded to ensure in-flight conditions. The green lines show the normalised frequency distribution of all data of the horizontal level runs used for flux measurements. The blue line represents the regression $\alpha = -1.856 + 10.449\frac{q_\alpha}{q_i}$.

slope. At the typical airspeed during measurements runs of 60m/s the offset corresponds to constant difference for the vertical wind speed of 3cm/s and the slope deviation translates directly to ~~an~~ a gain difference of 0.7%. Both figures are in the range of uncertainty of the results of the dedicated flight pattern.

From Fig. 6 we can furthermore see that the pitch variation during measurement runs are nearly Gaussian distributed, while the pressure ratio q_α/q_i is positively skewed due to the skewness of w at low level in a convective boundary layer (e.g. Hunt et al. , 1988).

3.3 Alignment of the 5-hole-probe and INS reference (beta-offset)

The angle of sideslip β is measured by the 5-hole-probe via the pressure difference q_β between the two holes in the horizontal plane. Then β is calculated by

$$\beta = \beta_0 + c_\beta \frac{q_\beta}{q_i} \qquad (12)$$

where β_0 is the alignment offset between the 5-hole-probe and the INS reference system and c_β in analogy to c_α (Eq. 8) a proportionality constant. For a symmetrical sonde in a pressure field undisturbed by the aircraft c_α and c_β would be identical, as e.g. Mühlbauer (1985) proved in a wind tunnel. But as we include in the calibration the influence of the aircraft pressure field which is not symmetrical with respect to the longitudinal axis of the sonde, c_α and c_β are different. The porportionality c_β should not change between campaigns, but β_0 needs to be recalibrated with each remounting of the noseboom. We use $c_\beta = 11.36$ as determined in the calibration flights of Cremer (2008) and confirmed by Drüe and Heinemann (2013). Based on the assumption that the wind be constant for the out and return flights ~~we calculate for each pair of legs~~ the wind components orthogonal to the track ($u_{\perp 1}, u_{\perp 2}$, after the coordinate system has been rotated to align with the track direction) should cancel out. Note that the coordinate system of the return flight is rotated by 180° and thus this component changes sign. A misalignment of the 5-hole-probe with the INS would then result in a residual of the sum of $u_{\perp 1} + u_{\perp 2}$. This residual can be referenced to the misalignment by

$$\beta_r = \text{atan}(0.5 \frac{u_{\perp 1} + u_{\perp 2}}{\text{TAS}_1 + \text{TAS}_2}) \tag{13}$$

as a residual offset for the beta angle. With the large number of return-track flights under different situations and on different days we can assume that possible wind changes are randomly distributed. Thus, the wind induced part of β_r should also be randomly distributed and cancel out when averaged over a sufficiently large number. We then manually iterate the beta-offset β_0 such that the average over all β_rs is minimised. For the AirMeth 2013 flights we find $\beta_0 = -0.604$. Mallaun et al. (2015) pointed out that a misalignment of the β angle should show in a correlation between the vertical wind velocity and the roll angle, as a misaligned sonde would be tilted up- or downward and thus produce a spurious vertical wind. Following their suggestion we ~~testet~~ tested for the alignment-corrected wind calculation $w \sim \text{TAS} \cdot \sin\Phi$ for $\Phi > 5°$ and $|w_g| < 0.1$m/s and could not find any correlation.

3.4 Static pressure precision

We can use the series of return track flights for an estimation of the precision of the static pressure measurement. As we have passed during the return-flight the same location (with about ±200 m lateral deviation), we can calculate a pressure difference along the track. This difference is composed of sensor uncertainties, height variation of the aircraft and atmospheric change. The height variation is accounted for by calculating the static pressure for a reference height h_{ref} by

$$p_{\text{ref}} = p_s + (h - h_{\text{ref}}) \frac{p_s g}{RT} \tag{14}$$

with p_s the static pressure (Eq. 6), g the acceleration due to gravity, R the gas constant for air and T the temperature. As reference height we define the mean over both flight legs. The atmospheric change is handled by this procedure: for each position along the track we have a

$$\Delta p = |p_{\text{ref2}} - p_{\text{ref1}}|, \tag{15}$$

the absolute value of the pressure difference between both passes, and in analogy a Δt, the time elapsed between both overpasses. Plotting Δp versus Δt shows increasing scatter with increasing Δt. A least squares fit gives ~~at the~~ with its ordinate offset at Δt=0 the remaining uncertainties of the sensors. We find this Δp_0 to be < 0.1hpa. This uncertainty estimate includes the uncertainty of the direct pressure measurement as well as that due to the aircraft height based on the gps GPS data. With this uncertainty a pressure gradient detection limit for a 100 km long leg would be 0.001hpa/km. Note that this method can only estimate the relative accuracy, a constant offset in the static pressure measurement cannot be detected.

3.5 Accuracy of the horizontal wind measurement

The difference in the mean wind speed $\Delta|U|$ between out and return legs as shown in Table 1 has over all 15 pairs a mean value of 0.08m/s and a standard deviation of 0.33m/s over all 15 pairs. This supports our assumption that $\Delta|U|$ mostly results from atmospheric variation and that the calibration and measurement uncertainty rather is of the order of 0.08m/s. Rotating the wind components in into an along track $v_{\|}$ and an across track $u_{\perp}$ component we get a mean difference in $v_{\|}$ of 0.11m/s which translates in a calibration uncertainty for the dynamic pressure of ≈ 0.09hpa and is of similar order as the estimate given in section 3.1. Calculating a Gaussian error propagation on the by far dominating term for the along track component

$$v_{\|} = v_{g\|} - \sqrt{\frac{2q_i RT}{p}} \tag{16}$$

using the uncertainties 0.1hpa for the static pressure p, 0.12hpa (averaging the estimates of Sections 3.1 and 3.5) for the dynamic pressure q_i, 0.1K for the temperature T, and 0.03m/s for the ground speed $v_{g\|}$ results in an uncertainty for $v_{\|}$ of 0.18m/s. In this estimate the uncertainty of q_i clearly dominates the other contributions by about one order of magnitude. Note that this estimate is valid for wind measurements during horizontal flight legs. The accuracy during turn manoeuvres, ascents and descents may be less. For the alignment offset between the 5-hole-probe and the INS we estimate the calibration uncertainty by the standard deviation of β_r, given in Table 1 (second last line) to be $0.05°$. Furthermore, applying the procedure described in section 3.4 to the horizontal wind components yields as uncertainty estimates for both components of 0.2 m/s as uncertainty estimate for both components, confirming the estimate in this section.

3.6 Methane analyser

The data aquisition system of Polar 5, DMS, and the methane analyser ran on autonomous computer system each with their individual clocks. They were synchronised by recording within the DMS an analogue output of the methane analyser. Section-wise cross correlation revealed that the analyser's clock ran typically 3.5e-5 $\cdot 10^{-5}$ slower than the DMS. This sychronisation was done individually for each flight leading to a timing accuracy of 0.01s between the systems.

After clock synchronisations, the time lag of the methane signal due to delay in the tubings was found by a cross-correlation analysis of the FGGA data with the vertical wind velocity for selected runs with clearly positive methane and humidity fluxes. Prior to the correlation analysis all signals were high-pass filtered with a cut-off at 0.1 Hz (corresponding to $\approx$ 600 m horizontal distance at 60 m/s). The time lags for CH_4, CO_2 and H_2O are 0.68s, 0.66s and 0.72s, respectively, with negligible variation between individual runs. Water vapour has a slightly larger delay due to interaction with the tubing. However, as Ibrom et al. (2007) have shown, for referencing the methane signal to a dry mole fraction the water vapour signal needs to be treated with the same time delay as the methane signal, as the actual condition in the measurement cell are is relevant. A correlation analysis between the FGGA and Vaisala humidity signals showed a delay of 0.36s of the Vaisala signal. The time delay of the methane signal due to the tubing was confirmed by ground a test. A step change of the concentration a the inlet took 0.5s to arrive at the analysers reading.

The cell pressure in the methane analyser is maintained to 140 Torr and shows little variation during level flux measurement runs. Desjardins et al. (2017) used a Picarro G2301-f in a Twin-Otter for flux measurements and found a weak correlation of the methane concentration with the cell pressure. We performed coherency and correlation analysis with spectral resolution and as integral statistics and could not find any correlation between pressure and the CH_4 signal. Also Wolfe et al. (2017) reported no pressure effect on the CH_4 signal from an airborne LGR analyser.

A specific, and especially arctic problem of airborne cavity ring down spectroscopy is sensor warm up. In a flux tower setup sensors typically run continuously, but for airborne applications the instruments can only be switched on after start of the engines. Occasionally sensors could be pre heated by ground power but this was not always available. Laboratory and in-flight tests showed, that the CH_4 concentration reported from a cold sensor increased with cavity temperature for ~~tempertures~~ temperatures lower than 34°C. For below-zero starting condition warm-up time was up to 45 minutes.

4 Accuracy of methane flux measurements

To analyse the accuracy of airborne trace gas flux measurements we estimate the flux detection limit, test the instrument precision and use a spectral analysis to compare methane fluxes with the well known behaviour of heat and moisture fluxes. We focus on the covariance at the height of the aircraft. For referencing the flux measurement to the surface level and footprint calculations we refer to Kohnert et al. (2017) and Serafimovich et al. (2018).

4.1 ~~Turbulent flux detection limit~~Instrumental noise

~~Following a method suggested by Wienhold et al. (1995)~~ To determine the instrumental noise level from our recordings we follow a method described by Mauder et al. (2013), based on the property of univariate white noise being uncorrelated with the signal. Thus it shows only in the 0-lag of the autocorrelation but not in further lags. The variance of the noise error ϵx^2 of a quantity x can be estimated as

$$\overline{\epsilon x^2} = C_{11}(0) - C_{11}(p \rightarrow 0)$$

where $C_{11}(0)$ is the autocorrelation of x at lag 0 and $C_{11}(p \rightarrow 0)$ the autocorrelation as a function of lag p extrapolated to lag 0. For the FGGA we get for CH_4 $\epsilon x = 0.0037$ppm, for CO_2 $\epsilon x = 0.695$ppm and for H_2O $\epsilon x = 34.9$ppm, all confirming the design specifications of the instrument. Applying the same proceedure to the data of vertical wind velocity and temperature we get for w: $\epsilon x = 0.029$m/s and for T$\epsilon x = 0.0022$K. For $C_{11}(p \rightarrow 0)$ we use the ~~cross-covariance function to estimate the~~ lags 3-20 corresponding to 0.16s to 1.0s sampling time.

4.2 Turbulent flux detection limit

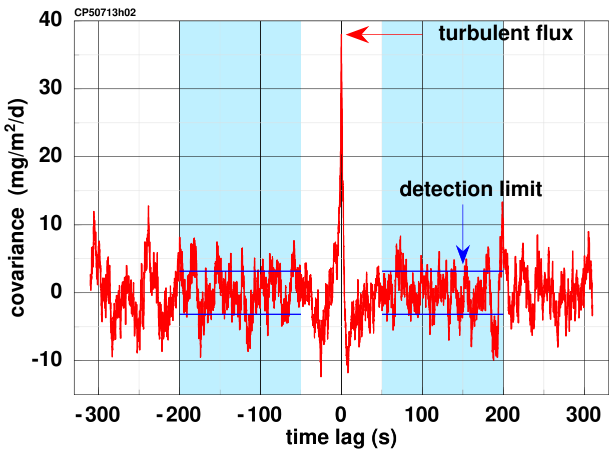

Figure 7. Example of the covariance function of w' and CH_4' versus time lag to illustrate the range used for estimation of the flux detection limit. The covariance is scaled to mg/~~d/~~m^2/d. Blue shaded areas indicate the ranges -200s to -50s and 50s to 200s over which the standard deviation has ~~be~~ been calculated~~to estimate~~ , it is marked by the ~~flux detection limit~~horizontal blue lines. At the typical airspeed of 60m/s the range corresponds to 3 to 12 km. The figure shows data of run CP50713h02 with a methane flux of 30.9mg/m^2/d (at lag zero, marked by the red arrow). The ~~flux detection limit~~ standard derivation over the blue marked range is 3.1mg/m^2/d, which is taken as estimate for the flux detection limit.

Next we determine the turbulent flux detection limit, now based on the property of the bivariate white noise being uncorrelated with the signal.

First, we use a method suggested by Wienhold et al. (1995) based on the cross-covariance function. Here, the correlation between biophysical (scalar abundance) and transport (air motion) mechanisms are removed by shifting the two time-series against each other, leaving only the random correlations attributed to instrumental noise. We calculate the standard ~~deviation~~ derivation of the cross covariance function for the time lag interval -200s to -50s and 50s to 200s. At a typical airspeed of 60m/s this corresponds to shifting the two time series by 3 to 12km horizontal distance. Figure 7 shows an example for a horizontal flight section on 2013-07-13, where the turbulent flux is marked at lag 0 and the estimate for the detection limit as desribed above by blue lines.

Applying this procedure to all horizontal flight legs of the 2013 campaign with positive methane, heat and moisture fluxes and negative ~~CO2~~ CO_2 fluxes and averaging we get detection limits of 3.9 mg/m^2/d for $\overline{w'CH_4'}$, 1.4 g/m^2/d for $\overline{w'CO_2'}$, 4.2 W/m^2 ~~/s~~ for the sensible heat flux and 8.8 W/m^2 ~~/s~~ for the latent heat flux.

~~Applying the Billesbach (2011) method~~ Billesbach (2011) provides an alternative "random shuffle" method for determining the turbulent flux detection limit: here the bivariate white noise property is achieved by re-calculating the eddy-covariance after one of the variables has been randomly "time-shuffled" instead of shifted. Applied to all 44 low level flight legs of the AirMeth 2012 North Slope campaign this method yields comparable flux detection limits of 4.9±1.4g/m^2/d 4.6±1.9W/m^2, 3.9±1.3W/m^2 and for the fluxes of methane, sensible and latent heat, respectively. The LGR ~~RMT 200~~FMA sensor installed in 2012 did not measure CO_2.

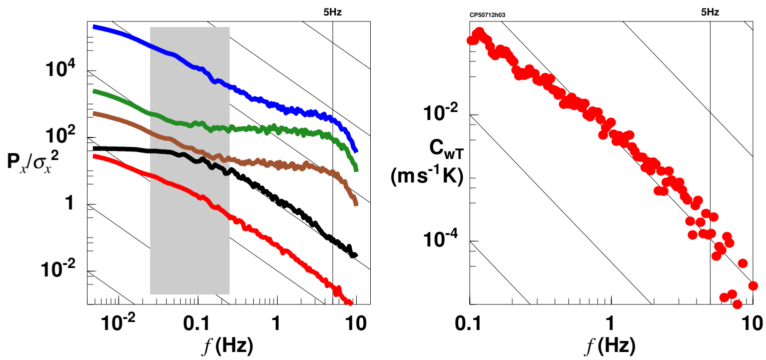

Figure 8. left: power spectra of the fluctuation of temperature (red), vertical wind velocity (black), CH_4 (brown), CO_2 (green) and water vapour mixing ratio (blue). The spectra are nondimensionalised by their respective variance and shifted in the plot by one decade increasingly. The sloped lines indicate a -5/3 decrease. The grey shaded area marks the scales corresponding from 5 z_i to $0.5z_i$, the range of dominant transport in a convective boundary layer. Right: covariance spectrum of vertical wind velocity and temperature. The sloped lines indicate -7/3 decrease. Data are from 2013-07-12, Alaskan North Slope, measurement height above ground 50 m, boundary layer height z_i=500m above ground.

4.3 ~~Precision~~

~~To determine the instrumental noise level from our recordings we follow a method described by Mauder et al. (2013), based on the property of white noise being uncorrelated with the signal. Thus it shows only in the 0-lag of the autocorrelation but not in futher lags. The variance of the noise error can be estimated as~~

$$\overline{\epsilon x^2} = C_{11}(0) - C_{11}(p \to 0)$$

~~where $C_{11}(0)$ is the autocorrelation of x at lag 0 and $C_{11}(p \to 0)$ the autocorrelation extrapolated to lag 0. For the FGGAwe get for CH_4 $\epsilon x = 0.0037$ppm, for CO_2 $\epsilon x = 0.695$ppm and for H_2O $\epsilon x = 34.9$ppm, all confirming the design specifications of the instrument. Applying the same proceedure to the data of vertical wind velocity and temperature we get for w: $\epsilon x = 0.029$m/s and for T$\epsilon x = 0.0022$K We use for $C_{11}(p \to 0)$ the lags 3-20 corresponding to 0.16s to 1.0s sampling time.~~

4.3 Spectral analysis

With the precision of ±3ppb for an integration time of 0.1s of the methane analyser we cannot expect to have spectral resolution of atmospheric fluctuations in the high frequency range that is comparable to temperature and vertical velocity. We examine power spectra (Figure 8) of a 100 km long flight leg at 50 m above ground. The measurement were taken on 2013-07-12 over the North Slope of Alaska in a convective boundary layer driven by a sensible heat flux of 70 W/m^2. The boundary layer height z_i was 500 m. Vertical wind velocity and temperature nicely follow a -5/3 drop off over nearly 2 decades for horizontal scales smaller than the boundary layer height. The data from the FGGA contain considerable white noise, most pronounced for CO_2, followed by CH_4 and least for the water vapour measurement. All three show too much HF-noise to resolve the inertial

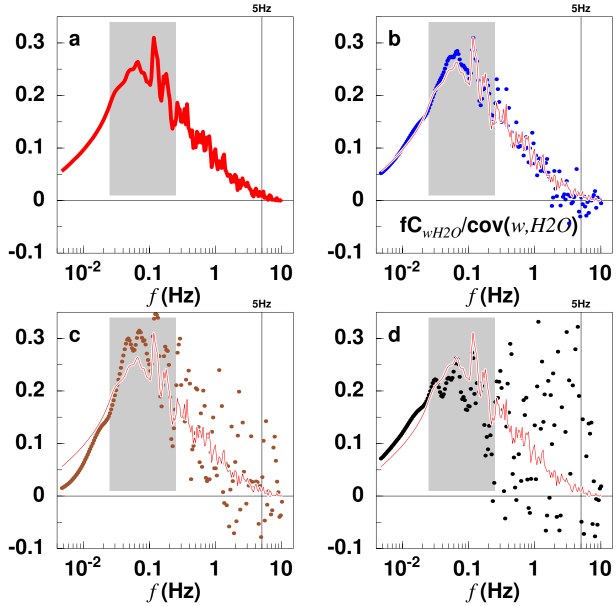

Figure 9. Cospectra normalised by their respective covariances. The data are from the same flight leg as in Figure 8. The grey shaded area marks the scales corresponding from 5 z_i to $0.5 z_i$. **a:** C_{wT} sensible heat flux, red, **b:** C_{wH2O} moisture flux, blue, **c:** C_{wCH4} methane flux, brown and **d:** C_{wCO2} flux of carbon dioxide, black. Note that normalisation by the covariance eliminates the sign. The first three fluxes are upward directed, the carbon dioxide flux is downward. For comparison C_{wT} is plotted as thin red line in b),c) and d).

subrange of turbulence. Similar results are shown by Wolfe et al. (2017) from low level airborne carbon flux measurements over Maryland and Virginia. Beyond about 5 Hz (corresponding to 12 m horizontal distance at the typical airspeed of 60 m/s) spectral drop off due to dampening in the tubing is visible. As w scales with the boundary layer height, power at the low frequency end does not increase further while the fluctuations in all scalars continue on scales far beyond 100 times the boundary layer height since the scalar quantities rather scale with their horizontal surface structure.

In the cospectrum of w and T we see the expected -7/3 drop off (e.g. Kaimal et al. (1972)), as shown in Figure 8. Beyond 5 Hz shows a small drop off, however, theses scales (corresponding to 12 m horizontal resolution) contribute a negligible amount to the covariance at the aircraft height of 50 m. The uncertainties at the low-frequency end are larger and more important for flux estimates.

Since the white noise of the trace gas analyser is uncorrelated with the vertical velocity it does not show in the covariance spectra (Figure 9). All 4 spectra are of similar shape. Although C_{wCH_4} and C_{wCO_2} have considerably more scatter in the high frequencies, their drop-off follows that of C_{wT}. Thus the turbulent vertical transport of trace gases is essentially identical to that of other scalars in the convective boundary layer.

Uncorrelated instrumental noise should vanish, or at least reduce, if measurements are repeated under similar conditions and averaged. The statistical error then reduces proportionally to $\frac{1}{\sqrt{n}}$, n being the number of independent realisations. We calculated covariance spectra for each of the 93 available low level legs of the 2013 AirMeth campaign, normalised by their

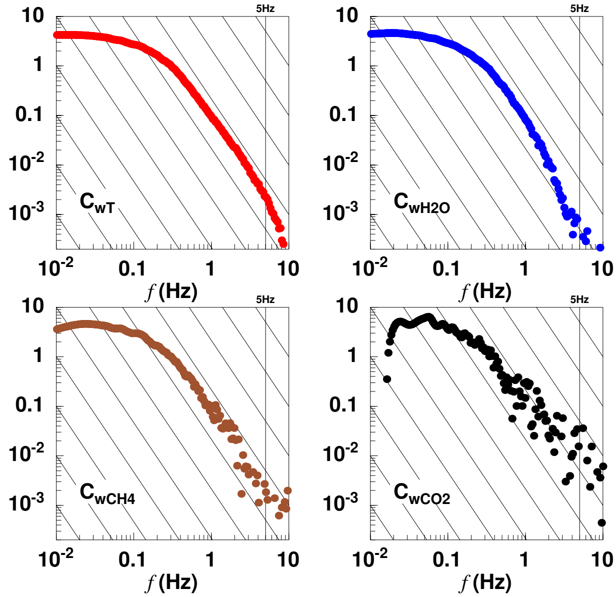

Figure 10. Stacked cospectra normalised by their respective covariances. The spectra are averages of ~~93~~ 87 horizontal flight legs totalling some ~~6000~~5600 km distance and ~~28~~26 h. **top left:** C_{wT} sensible heat flux, red, **top right:** C_{wH2O} moisture flux, blue, **bottom left:** C_{wCH4} methane flux, brown and **bottom right:** C_{wCO2} flux of carbon dioxide, black. Note that normalisation by the covariance eliminates the sign. Thin black lines show the -7/3 slope.

covariance and averaged. In these stacked cospectra (Figure 10) the expected -7/3 drop-off is reproduced for all 4 scalar fluxes~~.~~ ~~Again~~, again, with more scatter for the trace gases than for the water vapour or the temperature. Figure 10 shows that the instrumental noise leading to the spectral deviation in Figure 8 is uncorrelated with the vertical velocity and does not affect the covariance other than by a small increase of statistical uncertainty.

4.4 Dry mole fraction flux

We aim to determine the mass of methane being emitted from the surface per area unit and time interval. The trace gas analyser measures molecular ratios. As the atmospheric methane concentration is of a similar order as the density variation due to humidity fluctuations, the latter need to be taken in to account ~~when referencing~~ in computing a mass flux from the measured (wet) mole fractions ~~to a mass flux (Webb et al. , 1980)~~(Webb et al. , 1980).

A direct measurement of dry mole fractions requires gas drying. However, for eddy ~~correlation~~ covariance analysis a fast response of the system is very important. To keep the tubing as short as possible, we fed the outside air directly into the analyser avoiding delays by an air dryer, and account for the effect of humidity fluctuations by using fast humidity measurements. This method can even be applied in the tropics with considerably higher atmospheric humidity as Chen et al. (2010) have proven. To then find the dry mole fraction flux two options remain:

1: finding for each CH_4 sample taken in the measurement cell the exact humidity in the very same moment. For this method either an additional humidity measurement needs to be done in the analyser cell, or a separate fast humidity measurement can be referenced into the analyser with a high temporal accuracy.

2: calculating a wet mole fraction flux and applying what is commonly referred to as one of two WPL-correction terms (Webb et al. , 1980). For method **2** a separate humidity flux measurement needs to be available.

With the FGGA used in the 2013 AirMeth campaign the water vapour concentration is measured in the same air volume and at the same time as the trace gas concentration. Dry mole fraction can then be calculated by

$$\mathrm{CH}_{4d4} = \frac{\mathrm{CH}_{4w}}{(1 - \mathrm{mr}_{\mathrm{H_2O}})} \tag{17}$$

where $\mathrm{mr}_{\mathrm{H_2O}}$ is the ratio of water vapour to dry air. The dry mole flux then is

$$F = \overline{w'\rho'_{\mathrm{CH4}}}, \tag{18}$$

with ρ_{CH4} being the density of methane. We use these data to estimate differences and possible inaccuracies introduced by the above mentioned methods. We compare the dry mole fraction flux based on CH_{4d} with these $_4$ with the following four different methods:

A based on CH_{4w} plus the WPL-term calculated from the FGGA-humidity measurement.

$$F_A = \overline{w'\rho'_{\mathrm{CH4}w}} + \frac{m_a}{m_v}\left(\frac{\overline{\rho_{CH4}}}{\overline{\rho_a}}\right)\overline{w'\rho'_{v\mathrm{FGGA}}} \tag{19}$$

m_a/m_v is the mass ratio of dry air and water vapour, ρ_{CH4} and ρ_a the densities of methane and dry air, respectively, and $\rho_{v\mathrm{FGGA}}$ the water vapour density as measured by the FGGA. F and F_A should only be affected by numerical inaccuracies. The ratio F_A/F turns out to be 0.993±0.002.

B based on CH_{4w} plus the WPL-term taken from the Vaisala-humidity measurement.

$$F_B = \overline{w'\rho'_{\mathrm{CH4}w}} + \frac{m_a}{m_v}\left(\frac{\overline{\rho_{CH4}}}{\overline{\rho_a}}\right)\overline{w'\rho'_{v\mathrm{VAIS}}} \tag{20}$$

The ratio F_B/F turns out to be 1.041±0.035. The overestimation of 4.1% is due to the fact that the Vaisala measurement leads to a 31.2% larger humidity flux than the FGGA-measurement. However a direct comparison between averaged humidity measurements shows a good agreement. The flux difference is due to a different response behaviour of both sensors. Since in the 2012 campaign no other fast humidity measurement was available, this method had to be applied, leading to a slightly increased uncertainty of the methane flux. Assuming a similar behaviour for ~~2012 a siminlar behaviour~~ 2012 as for 2013, we ~~roughly 4% overestimation of~~ overestimate the methane fluxes by roughly 4%.

C based on $\mathrm{CH}_{4d\mathrm{vais}}$ as calculated from CH_{4w} and the in-cell humidity derived from the (outside) Vaisala measurement (HMT-330) referenced into the analyser cell. We calculated the mixing ratio from the relative humidity, temperature

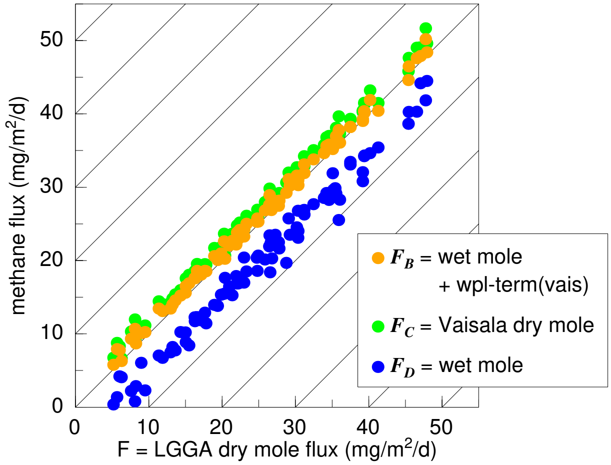

Figure 11. Comparison of different methods of accounting for humidity fluctuations in estimating methane flux from wet mole fraction measurements. The abscissa is the dry mole flux, F, Equation (18). Dark yellow is F_B, the wet mole flux plus WPL-term based on the Vaisala data according to Equation (20). Green represents F_C, Equation (21) and medium blue is the uncorrected wet mole flux, F_D, Eq.(22).

(Pt100) and the pressure and determined the time lag to the humidity measurement of the FGGA by a cross correlation of the high-pass filtered data to be 1.12 seconds and time shifted the data by this amount. Thus

$$\mathrm{CH}_{4d,\mathrm{vais}} = \frac{\mathrm{CH}_{4w}}{(1 - \mathrm{mr}_{\mathrm{vais,ref}})}$$

and the flux

$$F_C = \overline{w' \rho'_{\mathrm{CH_4 d,vais}}} \tag{21}$$

The ratio F_C/F turns out to be 1.080±0.047, somewhat larger than method **B** mostly due to the apparently insufficiently accurate time shift procedure. However, this method had to be used for the 2012 data (e.g. Kohnert et al. (2017)) to enable wavelet decomposition.

D no correction for water vapour

$$F_D = \overline{w' \rho'_{\mathrm{CH_4} w}} \tag{22}$$

The ratio F_D/F is 0.793±0.093. Thus, for our situation of methane emissions from arctic tundra the water vapour fluctuations lead to a flux under-estimation of 20% if not accounted for.

Figure 11 shows the above ~~described~~ for each horizontal flight section of the 2013 AirMeth campaign. We conclude, that even with a non-perfect humidity flux measurement, the dry mole fraction flux can be determined in polar regions with reasonable accuracy, in our case of the 2012 campaign an over-estimation of 4%.

5 Conclusions

We showed that aircraft are well suited tools to study methane emissions from Arctic tundra. The vertical fluxes of the most important greenhouse gases can be measured during low level flight legs with sufficient accuracy. We showed that a calibration of the essential coefficients of an aicraft turbulence equipment can be achieved with high accuracy by exploiting suitably arranged flux measurement legs. The natural variations in parameters (airspeed, pitch) due to manually controlled flights are sufficient. The horizontal wind components are measured with an accuracy better than 0.2m/s during level flight legs. The level of white noise of the trace gas analyser does not allow to resolve the inertial subrange of turbulent fluctuations of CO_2 and CH_4 with sufficient accuracy. However, since the noise is uncorrelated with the vertical wind velocity, the cospectra show a -7/3 drop-off if sufficient data are available for averaging. We found the detection limit of the methane flux to be about 4 mg/m^2/d and that of carbon dioxide to be about 1.4 g/m^2/d.

Appendix A: List of flight sections

A list of these pairs of flight legs is given in Table A1.

Acknowledgements. We thank the pilots, mechanics and engineers for their support. We thank Matthias Cremer for ~~helpful discussions~~ fruitful discussions and two anonymous reviewers for helpful comments. The AirMeth campaigns were fully funded by Alfred Wegener Institute Helmholtz Centre for Polar and Marine Research. This work has received funding from the Helmholtz Association of German Research Centres through a Helmholtz Young Investigators Group grant to T.S. (Grant VH-NG-821), and is a contribution to the European Union's Horizon 2020 research and innovation programme under grant agreement No. 727890, as well as to the Helmholtz Climate Initiative (REKLIM - Regional Climate Change). The National Ecological Observatory Network is a project sponsored by the National Science Foundation and managed under cooperative agreement by Battelle Ecology, Inc. This material is based upon work supported by the National Science Foundation [grant DBI-0752017]. Any opinions, findings, and conclusions or recommendations expressed in this material are those of the author and do not necessarily reflect the views of the National Science Foundation.

References

Baer, D.S., Paul, J.B., Gupta, M. and O'Keefe, A.: Sensitivity absorption measurements in a near-infrared region using off-axis integrated-cavity-output spectroscopy, Appl. Phys. B, 75, 261–265, doi:10.1007/s00340-002-0971-z, 2002.

Billesbach, D.P.: Estimating uncertainties in individual eddy covariance flux measurements: A comparison of methods and a proposed new method, Agric. For. Meteorol. 151, 394–405, doi:10.1016/j.agrformet.2010.12.001, 2011.

Bousquet, P., Ringeval, B., Pison, I., Dlugokencky, E.J., Brunke, E.G., Carouge, C., Chevallier, F., Fortems-Cheiney, A., Frankenberg, C., Hauglustaine, D.A., Krummel, P.B., Langenfelds, R.L., Ramonet, M., Schmidt, M., Steele, L.P., Szopa, S., Yver, C., Viovy, N., and Ciais, P.: Source attribution of the changes in atmospheric methan for 2006–2008, Atmos. Chem. Phys., 11, 3689–3700, doi:10.5194/acp-11-3689-2011, 2011.

Cambaliza, M.O.L., Shepson, P.B., Caulton, R., Stirm, B., Samarov, D., Gurney, K.R., Turnbull, J., Davis, K.J., Possolo, A., Karion, A., Sweeney, C., Moser, B., Hendricks, A., Lauvaux, T., Mays, K., Whetstone, J., Huang, J., Razlivanov, I., Miles, N.L., and Richardson, S.J.: Assessment of uncertainties of an aircraft-based mass balance approach for quantifying urban greenhouse gas emissions, Atmos. Chem. Phys., 14,9029–9050, 2014.

Chen, H., Winderlich, J., Gerbig, C., Hoefer, A., Rella, C.W., Crosson, E.R., Van Pelt, A.D., Steinbach, J., Kolle, O., Beck, V., Daube, B.C., Gottlieb, E.W., Chow, V.Y., Santoni, G.W., and Wofsy, S.C.: High-accuracy continuous airborne measurements of greenhouse gases (CO_2 and CH_4) using the cavity ring-down spectroscopy (CRDS) technique, Atmos. Meas. Tech., 3, 375–386, 2010.

Crawford, T.L., Dobosy, R.J. and Dumas, E.J.: Aircraft wind measurement considering lift-induced upwash, Boundary-Layer Meteorol., 80, 79–94, 1996.

Cremer, M.: Kalibrierung der Turbulenzmessonde der Polar 5, Dok.-Nr.mW-AWI-P5-2008-06, Messwerk, Braunschweig, Germany, 2008.

De Leo, R. V. and Hagen, F. W.: Aerodynamic performance of Rosemount model 858AJ air data sensor, Rosemount Report 8767, Aeronautical Research Department, Rosemount Inc., P.O. Box 35129, Minneapolis, Minnesota 55435 USA, 1976.

Desjardins, R.L., Wortha D.E., Pattey, E., VanderZaaga, A., Srinivasan, R., Mauder, M., Worthy, D., Sweeney, C. and Metzger, S.: The challenge of reconciling bottom-up agricultural methane emissions inventories with top-down measurements, Agric. For. Meteorol. 248, 48-59, https://doi.org/10.1016/j.agrformet.2017.09.003, 2017.

Dobosy, R., Sayres, D., Healy, C., Dumas, E., Heuer, M., Kochendorfer, J., Baker, B. and Anderson, J.: Estimating Random Uncertainty in Airborne Flux Measurements over Alaskan Turdra: Update on the Flux Fragment Method, J. Atmos. Oceanic Technol., 34, 1807–1822, 2017.

Drüe, C. and Heinemann, G.: A Review and Practical Guide to In-Flight Calibration for Aircraft Turbulence Sensors, J. Atmos. Oceanic Technol., 30, 2820–2837, doi: 10.1175/JTECH-D-12-00103.1, 2013.

Hartmann, J.: Airborne Turbulence Measurements in the Maritime Convective Boundary Layer, Ph.D. Thesis, Flinders University of South Australia, 163 pp., 1990.

Hiller, R.V., Neininger, B., Brunner, D., Gerbig, C. Bretscher, D., Künzler, T., Buchmann, N. and Eugster, W., Aircraft-based CH_4 flux estimates for validation of emissions from an agriculturally dominated area in Switzerland, J.Geophys.Res.Atmos., 119, 4874–4887, 2014.

Hunt, J.C.R., Kaimal, J.C. and Gaynor, J.E.: Eddy structure in the convective boundary layer – new measurements and new concepts, Q.J.R.Meteorol.Soc., 144,827–858, 1988.

Ibrom, A., Dellwik, E., Larsen, S.E. and Pilegaard, K.: On the use of the Webb–Pearman–Leuning theory for closed-path eddy correlation measurements, Tellus, 59B, 937–946, 2007.

Kaimal, J.C., Wyngaard, J.C., Yzumi, Y. and Coté, O.R.: Spectral characteristics of surface-layer turbulence, Quart. J. R. Met. Soc. 98, 563–589, 1972.

Karion, A., Sweeney, C., Pétron, G., Frost, G., Hardesty, R.M., Kofler, J., Miller, B.R., Newberger, T., Wolter, S., Banta, R., Brewer, A., Dlugokencky, E., Lang, P., Montzka, S.A., Schnell, R., Tans, P., Trainer, M., Zamora, R. and Conley, S.: Methane emissions estimates from airborne measurements over a western United States natural gas field, Geophys. Res. Lett., 40, 1-5, doi:10.1002/grl.50811, 2013.

Kohnert, K., Serafimovich, A., Hartmann, J. and Sachs, T.: Airborne Measurements of methane fluxes in Alaskan and Canadian Tundra with the Research Aircraft Polar 5, Reports on Polar and Marine Research, 673, 2014.

Kohnert, K., Serafimovich, A., Metzger, S., Hartmann, J. and Sachs, T.: Strong geologic methane emissions from discontinuous terrestrial permafrost in the Mackenzie Delta, Canada, Scientific Reports, 7, 5828, 2017.

Lee, M.F.: Dynamic response of pressure measuring systems, Technical Report 32, Department of Defence, Defence Science and Technology Organisation, Aeronautical Research Laboratory, Melbourne, Vic. Australia, April 1993.

Lenschow, D.H., Spyers-Duran, P.: Measurement techniques: Air motion sensing, NCAR Research Aviation Facility Bull. 23, 36 pp. [Available from NCAR, P.O. Box 3000, Boulder, CO 80307.], 1989.

Mallaun, C., Giez, A. and Baumann, R.: Calibration of 3-D wind measurements on a single-engine research aircraft, Atmos. Meas. Tech., 8, 3177–3196, 2015.

Mauder, M., Desjardins, R. L., and MacPherson, I.: Creating surface flux maps from airborne measurements: Application to the Mackenzie area GEWEX study MAGS 1999, Boundary Layer Meteorol., 129, 431-450, doi:10.1007/s10546-008-9326-6, 2008.

Mauder, M., Cuntz M., Drüe, C., Graf, A., Rebmann, C., Schmid, H.P., Schmidt, M. and Steinbrecher, R.: A strategy for quality and uncertainty assessment of long-term eddy-covariance measurements, Agric. Forest Meteor. 169, 122–135, doi:10.1016/j.agrformet.2012.09.006, 2013.

McGuire, A.D., Christensen, T.R., Hayes, D., Heroult, A., Euskirchen, E., Kimball, J.S., Koven, C., Lafleur, P., Miller, P.A., Oechel, W., Peylin, P., Williams, M., and Yi, Y.: An assessment of the carbon balance of Arctic tundra: Comparisons among observations, process models, and atmospheric inversions. Biogeosciences, 9, 3185–3204, doi:10.5194/bg-9-3185-2012, 2012.

Metzger, S., Junkermann, W., Mauder, M., Butterbach-Bahl, K., Trancón y Widemann, B., Neidl, F., Schäfer, K., Wieneke, S., Zheng, X. H., Schmid, H. P., and Foken, T.: Spatially explicit regionalization of airborne flux measurements using environmental response functions, Biogeosciences, 10, 2193-2217, doi:10.5194/bg-10-2193-2013, 2013.

Miller, S.M., Miller, C.E., Commane, R., Chang, R.Y.-W., Dinardo, S.J., Henderson, J.M., Karion, A., Lindaas, J., Melton, J.R., Miller, J.B., Sweeney, C., Wofsy, S.C., and Michalk, A.M.: A multiyear estimate of methane fluxes in Alaska from CARVE atmospheric observations, Global Biogeochem. Cycles, 30, 2016.

Mühlbauer, P.: Theoretische und experimentelle Untersuchungen zum Problem der Strömungsmessung mittels Fünf-Loch-Sonden an meteorologischen Forschungsflugzeugen der DFVLR, DFVLR Forschungsbericht DFVLR-FB 85-50, 128pp., 1985.

Rodi, A. R. and Leon, D. C.: Correction of static pressure on a research aircraft in accelerated flight using differential pressure measurements, Atmos. Meas. Tech., 5, 2569–2579, doi:10.5194/amt-5-2569-2012, 2012.

Saunois, M. Jackson, R.B., Bousquet, P., Poulter, B. and Canadell, J.G.: The growing role of methane in anthropogenic climate change, Environ. Res. Lett. 11, doi:10.1088/1748-9326/11/12/120207, 2016.

Sayres, D.S., Dobosy, R., Healy, C., Dumas, E., Kochendorfer, J., Munster, J., Wilkerson, J., Baker, B., and Anderson, J.G.: Arctic Regional Methane Fluxes by Ecotope as Derived Using Eddy Covariance from a Low Flying Aircraft, Atmos. Chem. Phys., 17, 8619–8633, doi:10.5194/acp-17-8619-2017, 2017.

Serafimovich, A., Metzger, S., Hartmann, J., Kohnert, K., Zona, D. and Sachs, T.: Upscaling surface energy fluxes over the North Slope of Alaska using airborne eddy-covariance measurements and enviromnental response functions, Atmos. Chem. Phys., submitted. doi:10.5194/acp-2017-1166, 2018.

Tjernström, M. and Friehe, C.A.: Analysis of a Radome Air-Motion System on a Twin-Jet Aircraft for Boundary-Layer Research, J. Atmos. Ocean. Tech., 8, 19–40, doi: 10.1175/1520-0426(1991)008<0019:AOARAM>2.0.CO;2, 1991.

Vellinga, O.S., Dobosy, R.J., Dumas, E.J., Gioli, B., Elbers, J.A. and Hutjes, R.W.A.: Calibration and Quality Assurance of Flux Observations from a Small Research Aircraft, J. Atmos. Oceanic Technol., 30, 161–181, doi: 10.1175/JTECH-D-11-00138.1, 2013.

Webb, E. K., Pearman, G. I. and Leuning, R.: Correction of flux measurements for density effects due to heat and water vapour transfer, Quart. J. Roy. Meteorol. Soc. 106, 85–100, 1980.

Wesche, C., Steinhage, D. and Nixdorf, U.: Polar aircraft Polar5 and Polar6 operated by the Alfred Wegener Institute, Journal of large-scale research facilities, 2, A87, doi: 10.17815/jlsrf-2-153, 2016.

Wienhold, F. G., Welling, M., and Harris, G. W.: Micrometeorological measurements and source region analysis of nitrous oxide fluxes from an agricultural soil, Atmos. Environ., 29, 2219–2227, 1995.

Wolfe, G. M., Kawa, S. R., Hanisco, T. F., Hannun, R. A., Newman, P. A., Swanson, A., Bailey, S., Barrick, J., Thornhill, K. L., Diskin, G., DiGangi, J., Nowak, J. B., Sorenson, C., Bland, G., Yungel, J. K., and Swenson, C. A.: The NASA Carbon Airborne Flux Experiment (CARAFE): Instrumentation and Methodology, Atmos. Meas. Tech. Discuss., https://doi.org/10.5194/amt-2017-398, in review, 2017.

Table A1. Horizontal flight legs used for the calibration of the dynamic pressure measurement and the alignment between the 5-hole-probe and the INS reference. The first column gives the code of the flight leg, further details and a full list of all flight legs of the AirMeth campaign 2013 is given in Kohnert et al. (2014). l is the leg length, h the height above ground, v_g the averaged ground speed, TAS is the averaged true air speed, t is the time needed to fly the legs, χ the true track angle, Ψ is the true heading, $\gamma = \Psi - \chi$ is the angle between heading and track, dd and ff is the wind direction and speed, u and v are the wind components (u positive to the East and v positive to the North), and $u_\perp$ and $v_\parallel$ are the components of the wind rotated to align with the track angle. All parameters are calculated after the calibration.

leg	l km	h m	v_g m/s	TAS m/s	t s	χ °	Ψ °	γ °	dd °	ff m/s	u m/s	v m/s	$u_\perp$ m/s	$v_\parallel$ m/s
CP507**06h02**	156	37	55.6	56.0	2830	96.8	96.8	-0.1	87.8	0.4	-0.4	-0.0	0.1	-0.4
CP507**06h03**	156	37	56.9	55.8	2768	276.3	276.0	-0.2	98.0	1.2	-1.2	0.2	0.0	1.2
CP507**11L08**	15	1212	62.0	64.3	240	181.5	175.5	-6.0	106.1	7.4	-7.1	2.0	7.1	-1.9
CP507**11L09**	9	1198	67.4	65.2	139	2.0	8.8	6.8	111.6	7.4	-6.9	2.7	-7.0	2.5
CP507**12h01**	90	51	66.3	56.4	1373	273.6	273.6	0.0	97.6	10.0	-9.9	1.3	0.7	10.0
CP507**12h02**	91	49	49.2	59.0	1866	93.3	94.8	1.5	99.0	9.8	-9.7	1.5	-1.0	-9.7
CP507**12h03**	96	52	48.3	57.9	2014	93.5	94.3	0.8	96.7	9.6	-9.5	1.1	-0.5	-9.6
CP507**12h04**	88	52	68.8	58.6	1292	273.5	272.9	-0.6	97.7	10.3	-10.2	1.4	0.8	10.2
CP507**19h01**	105	54	60.4	59.7	1750	338.8	342.1	3.3	81.7	3.5	-3.5	-0.5	-3.5	0.8
CP507**19h02**	115	55	58.8	59.3	1960	158.7	155.4	-3.2	75.5	3.4	-3.3	-0.8	3.3	-0.4
CP507**20h01**	97	51	57.3	58.2	1713	338.9	343.6	4.7	63.1	5.5	-4.9	-2.5	-5.5	-0.6
CP507**20h02**	105	54	60.0	59.7	1756	159.3	153.4	-5.8	62.1	5.2	-4.6	-2.4	5.2	0.6
CP507**20h03**	120	52	57.8	58.4	2088	330.2	332.3	2.2	50.0	3.0	-2.3	-1.9	-2.9	-0.5
CP507**20h04**	118	53	61.2	61.0	1938	150.1	146.6	-3.5	53.5	3.1	-2.5	-1.8	3.1	0.4
CP507**20h05**	69	52	58.4	59.5	1193	324.4	325.4	1.0	21.4	2.1	-0.7	-1.9	-1.7	-1.1
CP507**20h06**	69	52	61.6	60.6	1120	144.5	142.2	-2.3	24.8	2.2	-0.9	-2.0	1.9	1.1
CP507**20h07**	85	50	61.1	61.0	1403	301.1	302.8	1.8	34.9	2.8	-1.6	-2.3	-2.8	0.2
CP507**20h08**	83	50	60.7	61.2	1383	121.4	118.2	-3.2	38.6	2.9	-1.8	-2.3	2.9	-0.4
CP507**21L03**	12	1856	62.9	65.2	200	360.0	1.6	1.6	51.8	3.6	-2.9	-2.2	-2.9	-2.2
CP507**21L04**	13	1873	68.2	66.3	195	179.7	176.6	-3.0	52.0	3.3	-2.6	-2.0	2.6	2.0
CP507**21h01**	97	51	62.7	59.4	1555	179.9	178.8	-1.1	13.9	3.5	-0.8	-3.4	0.8	3.4
CP507**21h02**	68	78	63.0	66.3	1089	359.6	359.7	0.2	15.0	3.4	-0.9	-3.3	-0.9	-3.3
CP507**21h03**	96	79	68.5	65.3	1416	180.1	179.2	-1.0	15.1	3.3	-0.9	-3.2	0.9	3.2
CP507**21h04**	101	80	61.9	65.2	1645	359.8	359.8	-0.0	16.9	3.5	-1.0	-3.3	-1.0	-3.3
CP507**22h04**	70	55	67.3	62.8	1046	324.4	321.6	-2.7	174.7	5.3	-0.5	5.2	2.7	4.5
CP507**22h05**	68	51	56.0	60.4	1217	144.8	146.9	2.1	173.3	4.9	-0.6	4.9	-2.3	-4.3
CP507**23h02**	86	50	60.3	60.0	1437	211.9	216.7	4.8	307.1	5.4	4.3	-3.2	-5.4	0.5
CP507**23h03**	87	53	60.4	61.8	1457	32.0	27.0	-5.0	315.3	5.2	3.6	-3.7	5.0	-1.2
CP507**23h04**	116	52	61.8	60.6	1895	209.9	213.8	3.9	318.2	4.5	3.0	-3.3	-4.3	1.4
CP507**23h05**	108	53	61.3	62.8	1770	30.0	26.0	-4.0	317.3	4.5	3.0	-3.3	4.3	-1.3